Development of antisense RNA-mediated quantifiable inhibition for metabolic regulation

Ruihua Zhang, Yan Zhang, Jian Wang, Yaping Yang, Yajun Yan [*]

School of Chemical, Materials and Biomedical Engineering, College of Engineering, The University of Georgia, Athens, GA, 30602, USA

ABSTRACT

Trans-regulating elements such as noncoding RNAs are crucial in modifying cells, and has shown broad application in synthetic biology, metabolic engineering and RNA therapies. Although effective, titration of the regulatory levels of such elements is less explored. Encouraged by the need of fine-tuning cellular functions, we studied key parameters of the antisense RNA design including oligonucleotide length, targeting region and relative dosage to achieve differentiated inhibition. We determined a 30-nucleotide configuration that renders efficient and robust inhibition. We found that by targeting the core RBS region proportionally, quantifiable inhibition levels can be rationally obtained. A mathematic model was established accordingly with refined energy terms and successfully validated by depicting the inhibition levels for genomic targets. Additionally, we applied this fine-tuning approach for 4-hydroxycoumarin biosynthesis by simultaneous and quantifiable knockdown of multiple targets, resulting in a 3.58-fold increase in titer of the engineered strain comparing to that of the non-regulated. We believe the developed tool is broadly compatible and provides an extra layer of control in modifying living systems.

1. Introduction

Metabolic engineering was coined decades ago and has developed as an effective approach to manipulate cellular metabolism via biological and engineering tools (Stephanopoulos and Vallino, 1991; Bailey, 1991). Such an approach has largely facilitated the biosynthesis of various chemicals which were otherwise obtained inefficiently or unsustainably, with representative examples being natural products (Zhang et al., 2018) and biofuels (Sun et al., 2015). The central goal of metabolic engineering is to redirect, design and optimize metabolic routes for the desired outcome of cell factories. The conventional strategies such as gene overexpression and knockout of genomic targets converged metabolic flux successfully to a certain extent. While in more cases, the deletion of genomic targets is not feasible or optimal. Firstly, essential genes are indispensable for cell viability, and consist of a large portion of cellular genetic material (Baba et al., 2006). Secondly, due to the metabolic network complexity, the deletion of some non-essential genes can still impair cell functions in terms of biomass accumulation and energy balance. The concept of gene knockdown is thus introduced to achieve moderate or conditional inhibition. Moreover, as the biosynthesis process is coupled to changing cell status and environment conditions,

delicate control of cellular activities, such as dynamic regulation, has been reported superior to obtain high-performing cells (Shen et al., 2019). All these challenges have urged the devising of regulation tools to reliably tune cellular metabolic states.

Several methods of cellular regulation have thus been developed, many relied on RNA-based interactions. Noncoding RNAs (ncRNAs) have been widely used to post-transcriptionally inhibit gene expression *in trans* (Hebert et al., 2008; Yang et al., 2019; Cho et al., 2015; Lee and Moon, 2018). Among them, small regulatory RNAs (sRNAs) (Yoo et al., 2013) and antisense RNAs (asRNAs) (Nakashima et al., 2006) are of particular interest. The molecule structure of sRNAs consists of a target-binding sequence and a scaffold region for Hfq chaperone protein (Yoo et al., 2013), while asRNAs can function alone to interfere with mRNA expression. Although effective, most of their applications are optimized for strong regulation where inhibition rates are determined by ncRNAs intrinsic properties and the interaction with targeting molecules. Increasing evidence has suggested a fine-tuning necessity by experimental (Wang et al., 2017) and modeling studies (Tran et al., 2008). Moreover, such quantitative flux tuning data can improve modeling in return (Tan et al., 2011).

To date, several groups have reported inhibition rate studies towards

fine-tuning of metabolism by ncRNAs. While mostly focused on the 5′ untranslated region (5′ UTR) (Na et al., 2013; Park et al., 2014), a thorough study has not emerged to relate inhibition rates with such region in greater detail. Additionally, there also exist conflicts of ncRNAs length for efficient (Yoo et al., 2013; Na et al., 2013; Tummala et al., 2003; Wu et al., 2014; Jing et al., 2018) regulation that hinder easy adaptation. A representative work was conducted by Na and coworkers, where they designed synthetic sRNAs to regulate gene expression levels for cadaverine production in *Escherichia coli* (*E. coli*) (Na et al., 2013). Higher inhibition was observed when the sRNAs were used to target from ribosomal binding site (RBS) to intragenic loci. Similarly, the effect of sRNA targeting regions was studied by combining upstream of RBS, RBS and post-ATG sequences (Hoynes-O'Connor and Moon, 2016). However, only slightly varied inhibition rates were observed, possibly due to the coverage of most RBS nucleotides (nt) across all combinations. Such regions were also researched with asRNAs and high inhibition levels were determined by targeting the translation initiation region (TIR) (Park et al., 2014). The application of asRNAs with varied targeting loci has only been explored recently (Wu et al., 2014; Jing et al., 2018). Wu and coworkers designed asRNAs with approximately 30-nt step length to scan through 5′ UTR to modulate fatty acid pathway genes for naringenin biosynthesis in *E. coli*. Varied inhibition rates were obtained and used for combinatorial engineering without further characterization (Wu et al., 2014). A similar strategy was also used for the production of 1,2,4-butanetriol, where asRNAs were designed to target different post-ATG regions to obtain varied inhibition (Jing et al., 2018). Although effective, previous studies have not given explicit guidance for the design of inhibitory RNA molecules with differentiated efficiencies based on target-binding regions at single-base resolution.

In this study, we sought to further the systematic analysis of RNA-based inhibition tools and provide application-oriented information. We investigated the effect of target-binding length and region, the dosage between asRNAs and targets, and the comparison between asRNAs and sRNAs in inhibition tunability. Based on the results, we propose an asRNA-based tuning tool that targets 30-nt 5' UTR subregions to obtain quantifiable inhibition. To validate our observation and provide predictability, we constructed a mathematic model for inhibition levels based on competitive binding and refined binding energy terms. The developed asRNA tool was subsequently applied in a biosynthesis scenario of 4-hydroxycoumarin (4-HC) by regulating multiple genomic targets quantitatively. We believe the developed fine-tuning tool provides an additional layer of control in modifying living systems and is readily compatible with synthetic biology and metabolic engineering practices, as well as in RNA-based therapies.

2. Methods and materials

2.1. Media and chemicals

Luria-Bertani (LB) medium was used for strain reviving, inoculation and fluorescence assays. The modified minimal medium M9 (M9Y) was used for 4-HC fermentation containing (per liter) 20 g glycerol, 6 g Na_2HPO_4, 0.5 g NaCl, 3 g KH_2PO_4, 1 g NH_4Cl, 2 mM $MgSO_4$, 1 mM $CaCl_2$ and 5 g yeast extract. Standard chemicals including 4-HC, isopropyl β-D-1-thiogalactopyranoside (IPTG), ampicillin (Amp), kanamycin (Kan) and chloramphenicol (Cl) were purchased from Sigma-Aldrich unless otherwise noted. When added, Amp, Kan and Cl were used at the concentration of 100, 50 and 34 μg/mL, respectively. For the induction of pLlacO-1 promoter-based expressions, 0.5 mM IPTG was used. Phusion High-Fidelity DNA polymerase, restriction endonucleases and Quick Ligation Kit were purchased from New England Biolabs (Beverly, MA, USA). Plasmid Miniprep Kit, Gel Recovery Kit, and DNA Cleanup kit were purchased from Zymo Research (Irvine, CA, USA).

2.2. Strains and plasmids construction

E. coli XL1-blue (Stratagene) was used for plasmid construction and storage. *E. coli* BW25113 was used for inhibition measurements and 4-HC fermentation. *E. coli* BW25113 *hfq* knockout strain was purchased from the Keio collection strains (CGSC). Removal of its antibiotic resistance marker was conducted by electroporation of pCP20 plasmid into the cells (Datsenko and Wanner, 2000). Plasmids pZE12-luc, pCS27, pSA74 were used as the high-, medium-, and low-copy number plasmids with around 60, 25 and 3 copies, respectively (Lutz and Bujard, 1997). To construct the reporter plasmids, the expression operon of green or red fluorescent proteins (eGFP and RFP) (Cormack et al., 1996; Shaner et al., 2004) were inserted between *Acc*65I and *Bam*HI or *Xba*I sites of pZE12-luc, pCS27, pSA74, yielding pZE-GFP, pCS-GFP, pSA-GFP, pZE-RFP, pCS-RFP and pSA-RFP, respectively. Production plasmids pZE-EP-APTA and pCS-PS were from previous work in our lab (Lin et al., 2013; Shen et al., 2017). pZE-PT was constructed with pLlacO-1 promoter leading no RBS but two termini (PT) structures separated by a spacer sequence and used as the asRNA backbone plasmid (Nakashima et al., 2006; Yang et al., 2015). To construct plasmids containing shorter asRNAs (<50 nt targeting region), the targeting sequence was included in reverse primers. The forward primer was designed at ~80 nt upstream of the promoter, yielding PCR products of ~250 base pairs (bp). The PCR products were digested with *Aat*II and *Bam*HI which were introduced by the primers and ligated with likewise digested pZE-PT plasmid. For longer asRNAs, the targeting sequences were amplified directed using primers flanked with *Acc*65I and *Bam*HI sites that also exist between the two PT structures in pZE-PT plasmid. To construct sRNA-containing plasmids, RBS was first removed by amplification of Amp^R-pLlacO-1 sequences and ligated back to pZE12-luc between sacI and *Acc*65I, yielding pZE-RBSR. The MicC scaffold sequence was used to configure sRNAs (Yoo et al., 2013). The scaffold sequence was amplified from *E. coli* BW25113 genome using primers flanking the targeting regions and appropriate restriction sites. The PCR products and pZE-RBSR were ligated between *Hin*dIII and *Xba*I to generate the corresponding sRNA contained plasmids. The medium- and low-dosage plasmids were constructed by transferring the complete asRNAs or sRNAs units using the sacI-speI cloning region on pCS27 and pSA74. For targeting genomic genes (*fabD* and *ydiI*), their RBS sequences were extracted referred to the RBS calculator Version 2.1 (Salis et al., 2009), and then used to replace the native counterparts in pCS-GFP and pSA-GFP. The list of strain and plasmid details are included in Supplementary Table 1.

2.3. Optical and fluorescence assays

The quantification of cell density and fluorescence intensities was measured with Synergy HT microplate reader (BioTek). For measuring the cell density, cells were diluted 10 folds and 200 μl was loaded into 96 wells plates to read at optical density at 600 nm (OD_{600}). For fluorescence assays, the cells were transformed with corresponding plasmids and cultured in 3 mL LB medium with appropriate antibiotics at 37 °C and 270 rpm till OD_{600} reaches 1.0. Subculture was then conducted by adding 0.1% of the cultures into 3 mL fresh LB medium with 0.5 mM IPTG in addition to appropriate antibiotics. Cells were cultured at 37 °C and 270 rpm and taken out for measurements every 12 h. GFP intensity was measured by 10-fold dilution of the cell cultures and loaded into clear bottom 96 well plates with excitation wavelength of 485 nm and emission wavelength of 528 nm. RFP was measured similarly with excitation wavelength of 587 nm and emission wavelength of 610 nm. All fluorescence intensity results were normalized by respective cell growth (OD_{600}). Background fluorescence signal was subtracted for all measurements using control cell cultures without fluorescence proteins expression. The asRNA-mediated inhibition of GFP expression was

evaluated by the ratio of fluorescence between cells with and without asRNA targeting. All results were obtained with at least three biological replicates. Error bars indicate standard deviations of the presented results.

2.4. Fermentation conditions

For 4-HC biosynthesis, all transformants of BW25113 or its knockout mutants were cultured in 3 mL LB medium with appropriate antibiotics at 37 °C with shaking at 270 rpm for 12 h or overnight. Then 400 μL cultures were subinoculated (2%) into 125-mL baffled flasks containing 20 mL of M9Y media and cultivated with shaking at 270 rpm for 24–72 h. When needed, isopropyl β-D-1-thiogalactopyranoside (IPTG) was added to the medium during culture transfer with a final concentration of 0.5 mM. The culturing temperature was originally set at 37 °C. The timing for temperature switch to 30 °C and IPTG supplementation was coupled and studied as showed in the Results section. 1 mL cultures were sampled to measure cell density (OD600), mRNA levels and production profile by HPLC every 12 h with methods as described correspondingly.

2.5. Metabolite quantification

For quantification of 4-HC in fermentation broth, HPLC system 1260 infinity II (Agilent technologies) equipped with a reverse phase ZORBAX SB-C18 column and a 1260 infinity II Diode Array Detector WR was used. The oven and column temperature were both set at 25 °C. The mobile phase at a flow rate of 1 mL per min consisted of solvent A was formic acid (0.1% v/v) and solvent B was 100% methanol. The flowing gradient was as follows: 5–50% solvent B for 15 min, 50–5% solvent B for 1min and 5% solvent B for an additional 4 min. Quantification was based on the peak areas referring to the commercial standards at the wavelength of 285 nm. Titer analysis was conducted by comparing the sample reads with the standard 4-HC curve ($R^2 > 99.9\%$). All results were obtained with three biological replicates. Error bars indicate standard deviations of the presented results.

2.6. Mathematic model

The model was written in MATLAB R2019b. The equations were based on the law of mass action describing the interactions of the involved biomolecules. The detailed derivation and description of the model is presented in the Results section.

3. Results

3.1. Determining an efficient asRNA configuration

Although asRNA-based regulation has been broadly applied in metabolic engineering, the design principle is not explicit. Firstly, the characterization and application of asRNAs were mainly focused on the strong inhibition, which occurred when targeting the general 5' UTR region (Na et al., 2013; Park et al., 2014). However, asRNAs with defined efficacy can facilitate the in-depth modification of biological systems. Secondly, the length of effective asRNAs has been varied across reported studies, ranging from twenty to several-hundred nt (Park et al., 2014; Wu et al., 2014; Jing et al., 2018; Yang et al., 2015). Shorter asRNAs render flexibility in targeting at the cost of potential off-target effects, while longer asRNAs can lead to metabolic burden as well as challenges in strain construction. Determining an effective yet economical asRNA configuration will widely benefit future engineering efforts.

We sought to define an efficient asRNA design principle that can yield various inhibition levels on demand. We adapted the paired-termini structure of asRNAs as it was effective in our previous research (Yang et al., 2015). The functional asRNA sequence is flanked by a pair of inverted DNA repeats for enhanced stability. Initially, either the transcription initiation site (TIS) or the core RBS sequence from the common plasmid system (Lutz and Bujard, 1997) was set as the starts for asRNA targeting. We designed a series of asRNAs with binding sequence of 10–150 nt with 10-nt increments (Fig. 1a). The asRNAs were transcribed in high-copy number pZE12-luc plasmid to ensure their intracellular abundance. We first investigated the asRNA-mediated inhibition on pSA-GFP plasmid. When targeting from TIS, a cutoff length of 60 nt was observed
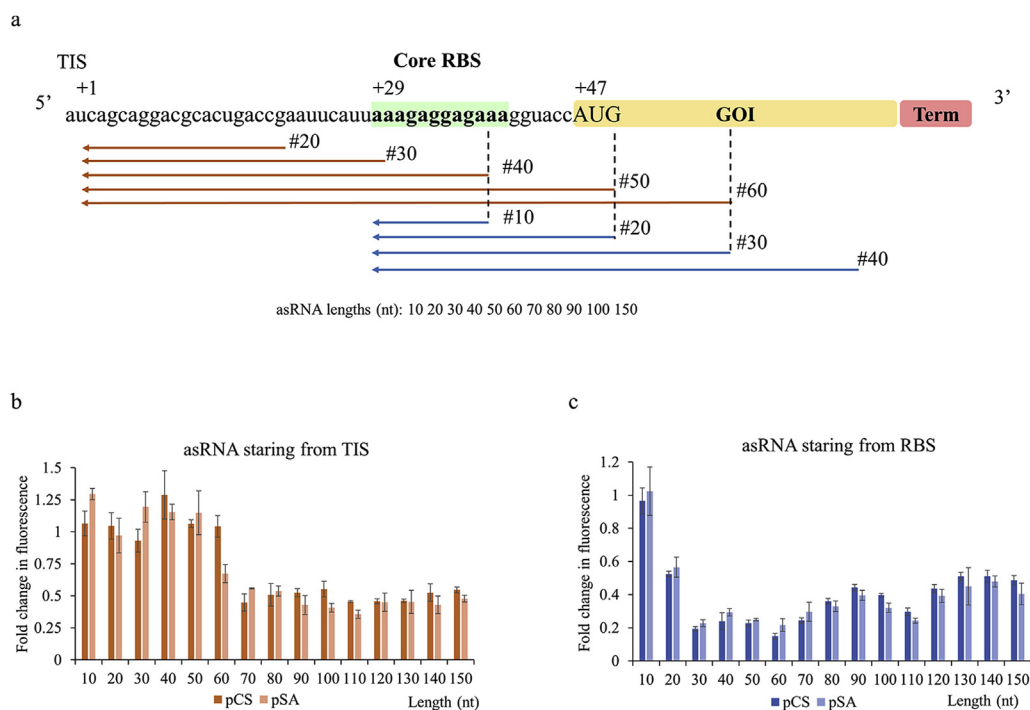

Fig. 1. Inhibition test of asRNAs on *egfp* expression from TIS or RBS with varied lengths. (a) Sequence layout of mRNA and asRNA targeting sequences. Arrows are demonstrative examples of asRNA targeting positions. (b) Inhibition results of asRNA from TIS (brown). (c) Inhibition results of asRNA from RBS (blue). Light bars indicate results for inhibition pSA-based expression (low copy number), dark bars for pCS-based expression (medium copy number). Y-axis indicates fold change of normalized fluorescence intensity comparing to the control. X-axis showed the targeting lengths of the asRNAs. (For interpretation of the references to colour in this figure legend, the reader is referred to the Web version of this article.)

for asRNAs to exhibit efficient inhibition. The 60-nt asRNA achieved 33% inhibition and the shorter asRNAs showed no significant effects on *egfp* expression (Fig. 1b). Meanwhile, 70-nt or longer asRNAs could inhibit the expression by around 50%. Interestingly, when targeting from RBS, the 20-nt asRNA showed 44% inhibition already and the 30-nt asRNA had further boosted inhibition of 77% (Fig. 1c). Longer asRNAs did not lead to higher but unstable inhibition levels. Using asRNAs to target mRNA from RBS was generally more effective than from TIS. These results confirmed that a 30-nt asRNA targeting RBS is sufficient and highly effective for gene regulation. Additionally, the same sets of asRNAs were used to regulate *egfp* expression on the medium-copy number pCS27 plasmid, and highly similar inhibition levels were observed (Fig. 1b and c), indicating minor dosage effect when asRNAs were relatively abundant. The inhibition tests were also conducted by targeting the *rfp* expression and yielded similar trends (Supplementary Fig. 1). Taken together, we determined an efficient 30-nt asRNA configuration that can yield varied inhibition levels in different conditions.

3.2. Characterization of quantifiable inhibition

We further investigated the potential reasons for the varied inhibition rates. In our genetic layout of expression cassettes, the distance between TIS and the start of core RBS is 29 nt, matching the difference of asRNA length cutoff between the results from TIS and RBS targeting tests. We therefore propose that the coverage of core RBS sequence, instead of the broader 5' UTR, is the main attribution to effective inhibition. Additionally, the ineffectiveness of the 30-nt asRNA targeting from TIS led to a further hypothesis that varied inhibition rates could be achieved by "walking" through the TIS-to-RBS region.

We thus designed a series of 30-nt asRNAs to map the inhibition rates over this abovementioned region (Fig. 2a). As expected, the inhibition rates increased while the asRNAs approaching the 12-nt core RBS (Fig. 2b). In the case of regulating *egfp* expression in the low-copy number plasmid, no inhibition was observed when less than 9 nt of the core RBS was targeted. Inhibition levels of 60% and 66% were achieved when 11 and 12 nt of the RBS sequence were targeted, respectively. The highest inhibition level of 79% was reached when the start of asRNA aligned with the start of core RBS (pZE-asRNA-#29), probably rendering the most effective hindrance to ribosome binding. As the targeting loci moving forward on the mRNA strand, inhibition levels decreased down to 64% when RBS was completely skipped. Additionally, *egfp* was expressed in high- and medium-copy number plasmids and similar gradient inhibition

levels were observed (Fig. 2b). The maximum inhibition level was 64% for the pZE-based expression, implying unsaturated asRNA levels under the equal-copy number condition.

To fully investigate the response range of varied inhibitions, we extended the targeting loci to the intragenic sequences, including both unstructured and structured regions based on the Mfold prediction (Zuker, 2003). The results showed that the 30-nt asRNAs were generally not effective (<25% inhibition) for both *egfp* and *rfp* expressed at low or medium levels (Fig. 2c and Supplementary Fig. 2). These results agreed with previous studies that short asRNAs could not effectively target loci within genes (Park et al., 2014). We reason that translation may be more difficult to be disrupted when RBS is free of asRNA interference, and structures of the coding sequences can jeopardize the asRNA efficacy. Nonetheless, we have identified a working range of the asRNA-based inhibition levels in the pre-gene region by varying RBS coverage. We also revealed the quantifiable inhibition in base-level resolution that can facilitate the controllable fine-tuning of metabolic flux.

Another interesting observation was that despite vastly different copy-numbers between the plasmids, the inhibition trends were similar when applying the same group of asRNAs (Fig. 1b and c). We hypothesize that the apparent inhibition rate of asRNAs is a combined result of target binding and relative dosages between asRNAs and the mRNA (assuming a constant abundance of intracellular ribosomes). We thus investigated the dosage effect by constructing asRNAs for *egfp* and *rfp* in the medium-copy number plasmid pCS27. These asRNAs were found ineffective towards high-expressed targets and less efficient for low-expressed targets (Supplementary Fig. 3). The expression of *egfp* and *rfp* on the pZE12-luc plasmid could only be inhibited by 3.5% and 21% using the most effective asRNAs, respectively. While targeting pSA-expressed e*gfp*, a gradient trend appeared with lower inhibition levels (Supplementary Fig. 3). Comparing to transcribing on the high-copy number plasmid, pCS-asRNA-#29 asRNA yielded 61% inhibition. And the other representative asRNAs pCS-asRNA-#9 and pCS-asRNA-#11 rendered 30% and 44%, respectively. These results confirmed that the relative dosage between asRNAs and the target needs to be carefully considered for desired inhibition levels. Moreover, quantifiable inhibition was proven feasible for different settings, while with varied efficiencies.

3.3. Comparison with the sRNA-based approach

In addition to asRNA-based post-transcription regulation, another effective ncRNA is sRNA, which requires a different assembly strategy
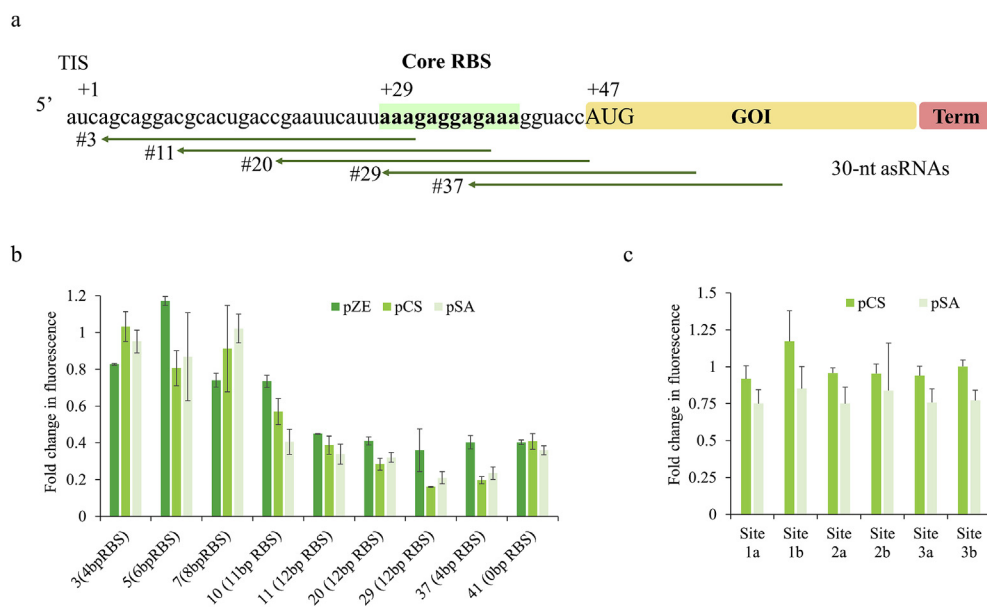

Fig. 2. Inhibition test of 30-nt asRNAs mapping from TIS or RBS. (a) Design scheme of asRNA walking. Arrows are demonstrative examples of asRNA targeting positions. (b) Inhibition rates related asRNA targeting regions. X-axis shows relative distance between TIS and asRNA start (numbers within parentheses indicate the length of core RBS covered). (c) Inhibition of asRNAs targeting sites within *egfp* gene. Dark green indicates high-expressed gene on pZE12-luc, green indicates medium-expressed gene on pCS27, light green indicates low-expressed gene on pSA74. Site 1a and 1b, 2a and 2b, and 3a and 3b are nearby regions, respectively. While 1b, 2b and 3b were prone to form secondary structures. The targeted sequences within GFP are annotated in the supplementary file. (For interpretation of the references to colour in this figure legend, the reader is referred to the Web version of this article.)
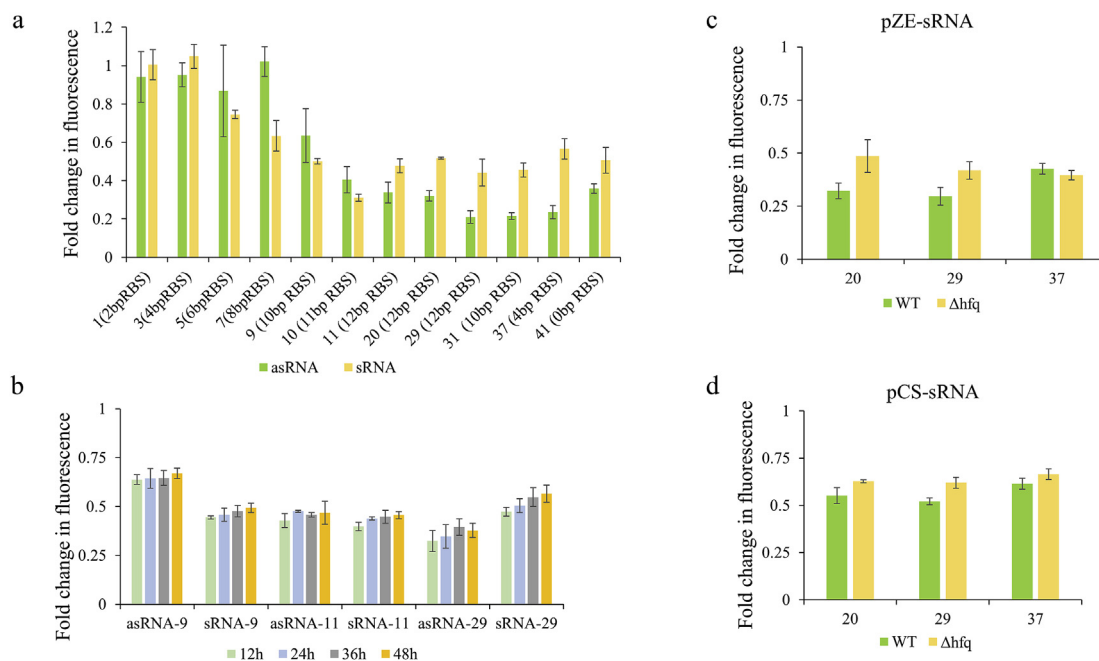
Fig. 3. Comparison of inhibition performance between asRNAs and sRNAs. (a) Comparison of inhibition between asRNA- and sRNA-based regulations on varied positions across 5′ UTR. X-axis shows relative distance between TIS and asRNA/sRNA start (numbers within parentheses indicate the length of core RBS covered). (b) Comparison of inhibition between asRNA- and sRNA-based regulations on the high-copy number plasmid at representative target sites over 48 h. (c) and (d) sRNA inhibition test in wild type (*E. coli* BW25113) and the corresponding *hfq* knockout strain.

with the aid of a chaperone protein Hfq (Yoo et al., 2013). In this section, we evaluated the effectiveness of our configuration by comparing to the sRNA-based approach. We first tested pZE-based sRNAs to inhibit pSA-GFP. Comparing to the asRNA results, sRNA-based inhibition to the same targets yielded a similar trend of increasing efficiency over the core RBS region (Fig. 3a). The sRNA-based regulation had a slight advantage when less core RBS nucleotides were targeted (pZE-sRNA-#5 to pZE-sRNA-#10). The highest inhibition level of 69% (pZE-sRNA-#10) was observed when 11 nt of RBS were targeted. However, sRNA-based inhibition suffered from an overall lower maximum efficiency of only around 50% (after pZE-sRNA-#10). Another aspect of evaluation is the long-term inhibition levels, as sRNAs were believed to be stable with Hfq-facilitated DNA binding (Yoo et al., 2013). We thus compared the inhibition of asRNAs and sRNAs with the same targeting regions for up to 48 h. In the case of high intracellular abundance, both groups were stable for the entire testing period with only slightly decrease in inhibition efficiency over time (Fig. 3b). Interestingly, when pCS-based ncRNAs were used, although both asRNA and sRNAs showed high stability over 48 h, sRNAs showed higher inhibition levels (Supplementary Fig. 4). We concluded that the long-term inhibition of asRNAs was stable comparing to sRNAs. We further investigated the effect of Hfq for sRNA-based inhibition by introducing highly active sRNAs in the *hfq* knockout strain. Comparing to the parental strain, Hfq removal led to different inhibition efficiencies. For pZE-sRNAs, 51% and 58% inhibition were observed for pZE-sRNA-#20 and pZE-sRNA-#29 in knockout strain, respectively. However, in wild type strains, around 70% of inhibition was obtained for both targets (Fig. 3c). The pCS-based test yielded similar results with overall lower inhibition due to less relative abundance of sRNAs (Fig. 3d). Although Hfq has been reported to play an important role in native sRNA-mediated mRNA repression and degradation (Aiba, 2007; Vogel and Luisi, 2011), our results indicated that it was not the determinant for synthetic sRNAs. Overall, comparing to the sRNA approach, our asRNA configuration showed a comparable regulation profile and higher efficiency over an extended cell lifespan. Additionally, given the complex interaction of Hfq with endogenous sRNA molecules, asRNAs may be an easier target for effective engineering towards tunable regulation.

3.4. A mathematic model for asRNA-mediated quantifiable inhibition

To better understand the outcome of the asRNA configuration, we constructed a preliminary mathematic model based on intracellular molecule interactions. We built the model considering the competitive binding between ribosome and asRNA molecules to the targeting mRNA, using thermodynamic equations. To generate this model, we applied the following assumptions:

Assumption 1. The cellular environment is homogenous.

Assumption 2. The interaction is at the equilibrium state when reporting signals were measured.

Assumption 3. Degradation of RNAs, proteins and their complexes are not considered in this model.

Assumption 4. There are no major interactions between asRNAs and ribosome.

Assumption 5. Each core RBS can bind at most one ribosome, or one asRNA each time.

Assumption 6. Bound mRNA-ribosome linearly reflects the reporting cellular functions.

Inspired by the observations from our experiments that asRNAs "walking" around the core RBS region render a gradient of inhibition efficiency, we further hypothesized that the inhibition rates can be described by separating 5′-UTR into subregions and assigning each an energy term, separated by the core RBS and the start codon (Fig. 4a). Specifically, the first potential asRNA-targeting subregion on 5′ is defined as pre-RBS subregion that contains the mRNA sequence from TIS up to the start of core RBS, providing a runway for ribosome landing, and therefore assumed to have low impact on translation initiation. The next subregion contains from core RBS to AUG, where ribosome interacts with most. The last subregion is the mRNA sequence after AUG, which assumed to have moderate impact on asRNA-mediated regulation. An asRNA covering a certain portion of each subregion would have a weighted sum of energy (ΔG_total), indicating its overall binding potential to the target mRNA. This hypothesis can be expressed in the following Eq. (Stephanopoulos and Vallino, 1991), where a, b and c are weighted coefficients. It is to our best knowledge the first attempt to quantitively describe the asRNA-mediated regulation *in silico* focusing on
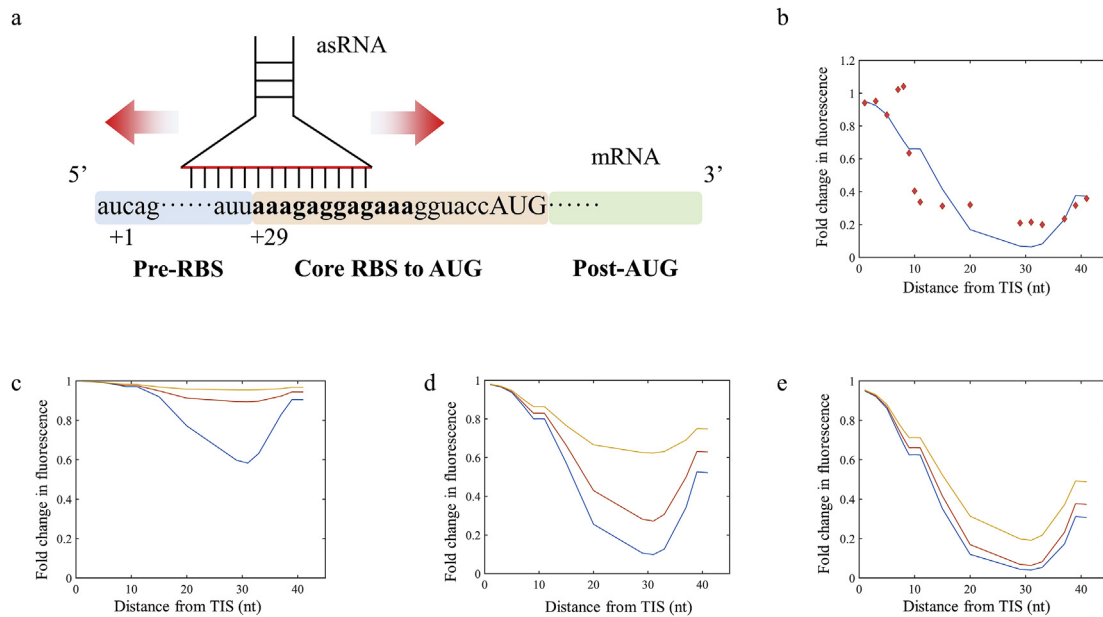
Fig. 4. The mathematic model for quantifiable asRNA inhibition. (a) Scheme of the proposed mechanism. (b) Plotting of experimental data with simulated inhibition levels for plasmid-originated RBS. Red diamonds indicate data points, blue lines indicate simulated results. (c)–(e) Simulated results for dosage effect. Blue, red, and yellow lines indicate targeted genes on low-, medium, or high-copy number plasmids, respectively. (c) Low copy number of asRNAs. (d) Medium copy number of asRNAs. (e) High copy number of asRNAs. (b)–(e) X-axis shows the relative distance between TIS and start of asRNA sequence. Y-axis shows fold change of reporting signal based on nonregulated control. (For interpretation of the references to colour in this figure legend, the reader is referred to the Web version of this article.)

the core RBS. And according to our hypothesis, coefficient b shall have the highest value, while a the least, indicating their corresponding contributions.

$$\Delta G\_total = a * \Delta G\_pre + b* \Delta G\_core + c* \Delta G\_post \tag{1}$$

The individual ΔG terms (ΔG_pre, ΔG_core and ΔG_post) were calculated based on the Nearest-Neighbor thermodynamic parameters (Chen et al., 2012). The specific binding potential of a certain asRNA to its target mRNA can be estimated using Eq. (Bailey, 1991), where ΔG is the binding energy of ribosome to a specific RBS or ΔG_total in the presence of asRNAs, and μ is an adjusting coefficient subject to data fitting. R is gas constant. T is Kelvin temperature set as 310 (~37 °C).

$$K = \mu * e^{-\Delta G/RT} \tag{2}$$

The mathematical model was based on the Law of mass action describing the interactions of the involved biomolecules. In the absence of asRNAs, the rate of mRNA-ribosome complex formation can be expressed using the Eq. (Zhang et al., 2018), where M, R and MR_control are the intracellular concentrations of free mRNA, free ribosome and mRNA-ribosome complex, respectively:

$$\frac{d[MR]}{dt} = ka*[M]*[R] - kd*[MR\_control] \tag{3}$$

We assume that the equilibrium has been reached for the interactions at the time of sampling (12 h or otherwise noted), thus Eq (Zhang et al., 2018). becomes:

$$\frac{kd}{ka} * [MR\_control] = KR * [MR\_control] = [M]*[R] \tag{4}$$

where KR is the binding coefficient for mRNA complexing with ribosome, which can be estimated by applying Eq. (Bailey, 1991) after obtaining specific ΔG numbers for ribosome-mRNA assembly from the RBS Calculator Version 2.1 (Salis, 2011).

Similarly, when asRNAs are involved, equilibrium can be reached for both mRNA-ribosome and mRNA-asRNA complexes, and all molecules are subject to their mass equations.

$$KR * [MR\_asRNA] = [M]*[R] \tag{5}$$

$$KA * [MA] = [M]*[A] \tag{6}$$

MR_control refers to mRNA-ribosome complex in the presence of asRNAs. Since the expression of genes is associated with the translated mRNAs upon binding of ribosomes, we define the inhibition index I by the ratio of expression levels between with and without asRNAs, thus the apparent signals for the reporting cellular functions can be expressed as below:

$$I = [MR\_asRNA] / [MR\_control] *100\% \tag{7}$$

The intracellular ribosome concentration was estimated by 20,000 ribosomes in 1 fL of *E. coli* cell volume (Bremer and Dennis, 1996; Gilbert, 2009). The relative abundance of total mRNA and asRNAs were estimated by plasmid copy numbers reported previously and the synthesis rate of 0.3 mRNA s^{-1} for a single copy gene for 12 h (Lutz and Bujard, 1997). The binding energy of ribosome to the specific RBS (ΔG = −3.83 kcal mol^{-1}) from our plasmid collection was reported by the RBS calculator Version 2.1 (Salis, 2011). As per the fitting process, we used the results of pZE-asRNAs targeting the pCS-GFP reporting plasmid and determined their copy number to be 60 and 25, respectively. We fixed the value of a to be 0.01 and searched for optimized values for μ, b and c using the Least-square method.

The training of our model based on the pZE-asRNAs targeting pCS-GFP returned values of b and c being 0.0248 and 0.0146, respectively. As the simulation showed, our model fitted well with the experiment results (Fig. 4b). Effective inhibition occurred when asRNAs were farther than 10 nt after TIS, when covering the intact core RBS. Highest inhibition levels were reached when asRNAs covered the core RBS and the following sequences on 3'. As asRNAs continued walking to exit core RBS on 3', inhibition levels started to decrease. The simulation and experimental results together showed the quantitative property of asRNA-based translation regulation. Moreover, since the coefficients b and c would be introduced in Eq. (Bailey, 1991), they weighted 1194% and 431% over a, respectively, confirming our key hypothesis that inhibition rates can be quantified by the weighted asRNA coverage around the core RBS subregion.

Using the returned coefficients, we also simulated the inhibition by different dosages of asRNAs and targets. The overall inhibition profiles were highly consistent with experimental results whenever applicable. When simulating asRNAs on the high-copy number plasmid, high inhibition levels were achieved for all dosages of the target, matching the experimental results (Figs. 2b and 4e). By lowering the asRNA dosage to medium, varied inhibition levels were simulated (Fig. 4d), and were also consistent with results that pCS-asRNA were not able to inhibition targets with high dosages effectively (Supplementary Fig. 3). Additionally, we simulated scenarios with asRNAs on the low-copy number plasmid and found they could only inhibit low-dosage targets (Fig. 4c). The dosage simulation of asRNA-based inhibition confirmed our experimental results that asRNAs needs to be at least equally abundant to render effective inhibition.

3.5. Validation of the quantifiable inhibition using genomic targets

Given the prevailing existence of RBS in living systems, we vision this phenomenon of asRNA-based quantifiable inhibition to be broadly observed for genomic targets, while our developed model can be used to depict or even predict such observation to a certain extent. To this end, we designed a series of asRNAs to quantifiably regulate two *E. coli* genes (*fabD* and *ydiI*) *in vivo*. We selected *fabD* and *ydiI* as the genomic targets due to their significant inhibitory impact on the biosynthesis of 4-HC. The resultant asRNA-mediated inhibition profiles were then used to validate the developed mathematic model with the return coefficient values from training.

To demonstrate the quantifiable inhibition, we extracted the 5′-UTR genomic fragments of *fabD* and *ydiI* to replace the standard RBS sequence on the pCS27 plasmid, yielding pCS-fabD-GFP and pCS-ydiI-GFP, respectively. The translational strength of genomic 5′-UTR sequences were weaker than the standard, while putting them on the medium-copy number plasmid pCS27 ensured sufficient *egfp* expression upon induction (Supplementary Fig. 5). The replacing 5′-UTR sequences consisted of the potential RBS and an additional 30 nt on 5′ to restore genomic conditions

and to provide room for asRNA walking (Fig. 5a). The potential RBS sequences were identified by using sequentially truncated 5′ sequences as the inputs for the RBS Calculator Version 2.1 (Salis et al., 2009). The sequence cutoff was then determined when observing a decrease in predicted translation initiation rate. A series of asRNAs were then designed and transcribed on the pZE12-luc plasmid for inhibiting the expression of *egfp* on pCS-fabD-GFP and pCS-ydiI-GFP, respectively. In both cases, varied inhibition rates were observed (Fig. 5b and c), spanning from low to high levels (up to 80%), providing a working range of quantifiable inhibition. For targeting pCS-fabD-GFP, asRNAs started to exhibit repression when the 5′ end of core RBS is met (19% for pZE-asRNA-f19). Extended coverage of the *fabD* core RBS improved the asRNA-mediated inhibition to around 80% for pZE-asRNA-f21 and pZE-asRNA-f25 (Fig. 5b). Similar trend was observed for asRNAs repressing pCS-ydiI-GFP (Fig. 5c). Cells co-transformed with pZE-asRNA-y45 showed low inhibition of 25%, when only 2 nucleotides of the *ydiI* core RBS was targeted. By asRNAs walking towards 3′ end, higher inhibition levels could be observed (up to 64% with pZE-asRNA-y51). The experimental results were highly consistent with the results of asRNAs targeting the standard RBS, implying this quantifiable inhibition broadly exists. Upon identification of core RBS, asRNAs with varied inhibition levels can be designed and used to finely regulate cellular functions.

Using the experimental inhibition profile for the genomic RBS, we sought to validate the developed model based on the returned coefficient values from training. The values of ΔG_total were calculated by determining the core RBS sequences (Fig. 5a) using the Nearest-Neighbor thermodynamic parameters (Chen et al., 2012). The binding tendency (ΔG) between ribosome and specific 5′ UTR sequences for the genomic targets were estimated (-4.87 kcal mol^{-1} for *fabD* and -1.83 kcal mol^{-1} for *ydiI*) by the RBS Calculator Version 2.1 (Salis et al., 2009). The simulated results with the experimental inhibition profile were directly compared for model validation. As the results showed (Fig. 5b and c), our model independently described the range of targeting loci exhibiting significant inhibition gradients for both genomic targets.
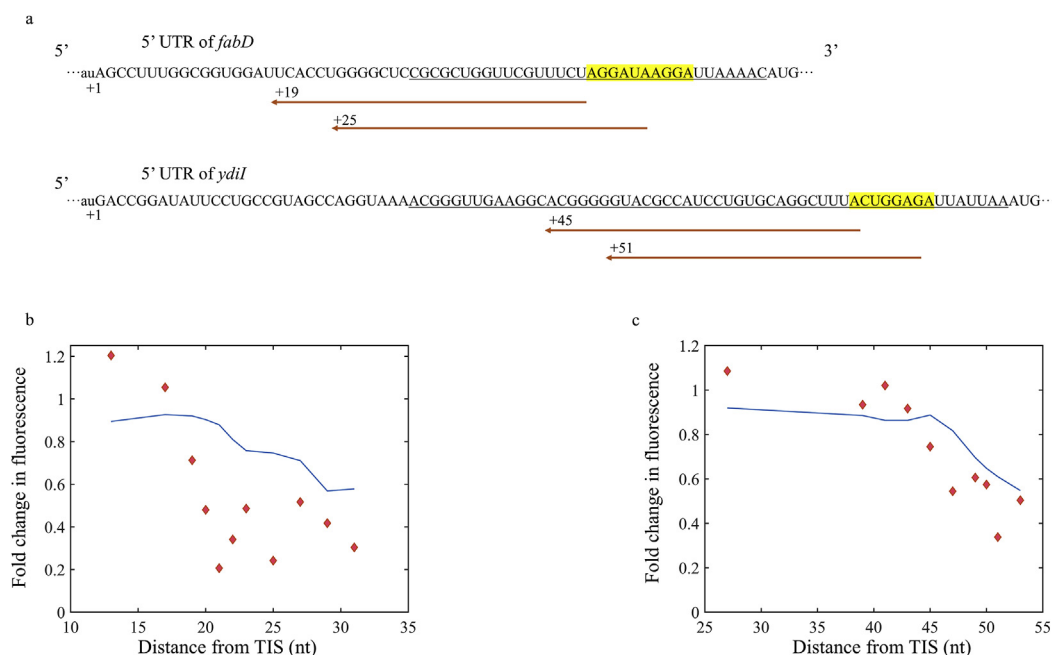
Fig. 5. Targeting 5′ UTR from genomic targets using quantifiable asRNAs. (a) Sequences of extracted 5′ UTR for *fabD* and *ydiI*. The underlining nucleotides are identified translation-relevant sequence by the RBS calculator Version 2.1. Yellow-highlighted nucleotides are assumed core RBS. The brown arrows under each 5′ UTR sequence are demonstrated asRNAs, with relative distance to TIS displayed. (b) Plotting of experimental data with simulated inhibition levels for asRNAs targeting pCS-fabD-GFP. (c) Plotting of experimental data with simulated inhibition levels for asRNAs targeting pCS-ydiI-GFP. (b)–(c) X-axis shows the relative distance between TIS and start of asRNA sequence. Y-axis shows fold change of reporting signal based on nonregulated control. (For interpretation of the references to colour in this figure legend, the reader is referred to the Web version of this article.)

3.6. Application of quantifiable and simultaneous knockdown of fabD and ydiI for 4-HC biosynthesis

An important scenario for applying gene knockdown is in the biosynthesis of valuable chemicals by tuning the metabolic behavior in cells. While the recent attempts to use asRNAs with different inhibition levels has been reported (Wu et al., 2014; Jing et al., 2018), this is to our best knowledge the first study to obtain and apply quantifiable asRNAs from an explicit designing mechanism. As we observed a gradient of inhibition levels on the 5' UTR of *fabD* and *ydiI*, asRNAs with high, medium and low efficiency were selected for regulating genomic expression of *fabD* and *ydiI*, respectively. For *fabD*, pZE-asRNA-f19, pZE-asRNA-f20 and pZE-asRNA-f21 were selected with 19%, 52% and 79% inhibition rates, respectively. While for *ydiI*, pZE-asRNA-y45, pZE-asRNA-y50 and pZE-asRNA-y51 were selected with 25%, 43% and 64% inhibition rates, respectively (Fig. 6b). To investigate the potential crosstalking of asRNAs targeting non-desired genomic genes, we applied the asRNAs for the counterpart target. As the results showed (Fig. 6b), most asRNAs did not show apparent inhibition on counterpart targets, except for pZE-asRNA-y45 exhibiting 16% repression on pCS-fabD-GFP. Although core RBS is a conservative sequence, the difference between genomic RBS sequences and that among the intact asRNA sequences seemed to disfavor the off-target interaction. It was also confirmed *in silico* by applying primer binding criteria for all asRNAs used in this section, that there was no nonspecific binding of asRNAs throughout the *E. coli* K-12 genome.

Next, we sought to use these asRNAs with quantified efficiency for multiplexed regulation of cellular metabolism, using the biosynthetic pathway of 4-HC as a demonstration. 4-HC is a valuable product whose de novo biosynthesis has been demonstrated in our previous work (Lin et al., 2013; Shen et al., 2017). To increase titer, attempts of strain engineering has been made to show that deletion of the 1,4-dihydroxy-2-naphthoyl-CoA hydrolase encoding gene *ydiI* was effective, however at the cost of impaired cell viability (Shen et al., 2017). Moreover, redirecting metabolic flux from fatty acid-branched product has significant contribution on malonyl-CoA availability for biosynthesis, such as inhibiting an essential gene *fabD* encoding [acyl-carrier-protein] *S*-malonyltransferase in *E. coli* (Yang et al., 2015). To demonstrate the quantifiable effect of metabolic regulation, we conducted 4^2 factorial experiments by introducing these asRNAs to (as well as a nonsense

asRNA control) along with the biosynthetic genes. The 4-HC biosynthesis pathway is shown in Fig. 6a, where *entC*, *pchB*, *sdgA* and *pqsA* are the key genes, and *aroL*, *tkaA*, *ppsA* and *aroG* (APTA) consist of a boosting module to increase chorismate availability (Lin et al., 2013).

When only introducing the key enzymes (pCS-EPPS), the presence of asRNAs targeting either gene with low-to-high inhibition levels increased the production of 4-HC (Fig. 6c). The unregulated strain produced 35 mg/L 4-HC at 24 h. When *ydiI* inhibition level was moderate (25% or 43%), varying *fabD* inhibition level has little effect on biosynthesis, although showing up to a 2.05-fold increase comparing to the control. When *ydiI* was inhibited at the high level or not regulated, we observed highly varied titers correlating to *fabD* inhibition levels. The highest titer was achieved when both targets were inhibited at high levels, resulting in up to a 3.58-fold increase, reaching 125 mg/L. We concluded that to achieve efficient biosynthesis of 4-HC, both *fabD* and *ydiI* needs to be highly inhibited, while varying *fabD* inhibition level has more influence on the cellular response. The "valley" shape of titers when *ydiI* was less inhibited may result from a trade-off effect between strengthened biosynthesis and the metabolic burden imposed by inhibitory asRNAs.

To further improve 4-HC biosynthesis, we introduced the APTA module to conduct the factorial experiment. The overall titers were largely increased (up to 525 mg/L), and all regulated strains showed superior performance than the unregulated control at 268 mg/L (Supplementary Fig. 6). The regulation effect by inhibiting *ydiI* was observed for all levels of *fabD* inhibited strains. However, different inhibition levels of asRNAs on *fabD* showed a weakened regulation effect. Generally, high titer of 4-HC was achieved when both *fabD* and *ydiI* was inhibited at the medium-to-high levels. Our results clearly showed the relevance between asRNA inhibition levels and metabolic regulation. Although the biosynthesis profile also suggested complex interactions of metabolite flow which pose a challenge to rationally engineering cellular functions, we believe the quantitative investigation of asRNA inhibition provides further information and enabled tools on our end to study biological systems with added accuracy and efficiency in future.

4. Discussion

The asRNA-based regulation has broad application scenarios such as synthetic biology, metabolic engineering and RNA therapy. We
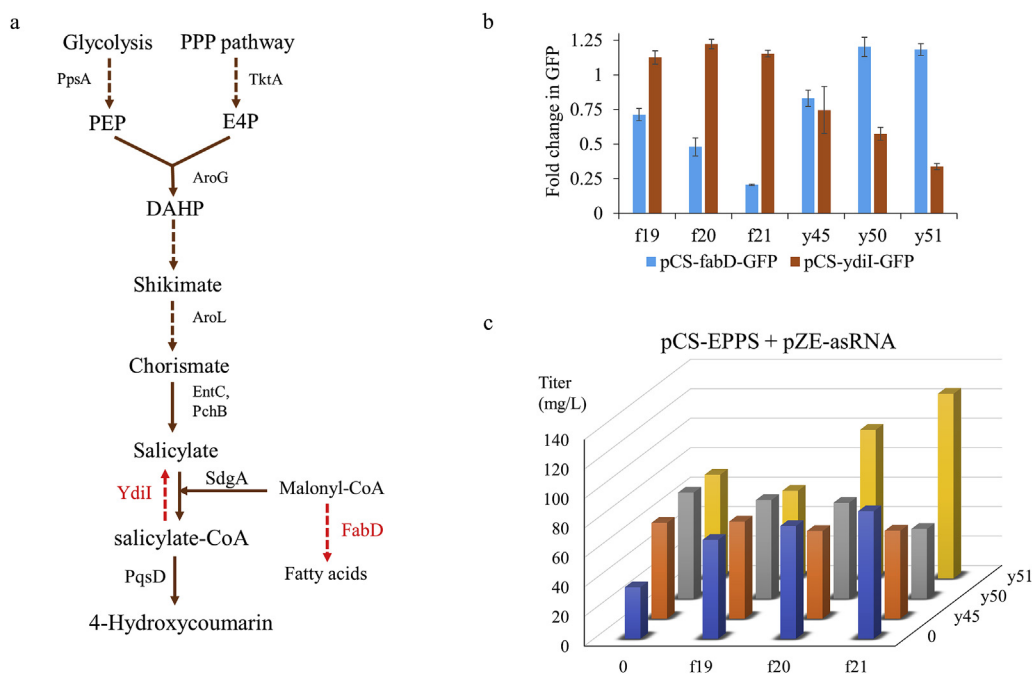

Fig. 6. Biosynthesis of 4-HC by multiplex inhibition of genomic targets by quantifiable asRNAs. (a) The biosynthesis pathway of 4-HC from glycolysis and the pentose phosphate pathway (PPP). Only overexpressed or regulated enzymatic steps are labeled. FabD and YdiI are enzymes encoded by the genes subjecting to asRNA-mediated regulation. (b) Specific and potential off-target inhibition by the quantifiable asRNAs on the genomic targets. (c) Results of 4-HC titer from pCS-EPPS and asRNAs on high level. Z-axis shows 4-HC titer after 24 h. X- and Y-axis show the corresponding asRNA plasmids used in the strains. 0 means strains transformed with the plasmid with nonsense asRNA control.

comprehensively and quantitively studied the asRNA-based inhibition towards different expression setups with varied asRNA length, targeting site and dosage. We determined a 30-nt asRNA configuration that is efficient and specific. Based on our results, the most effective inhibition occurs when the core RBS sequence is completely covered, while targeting part of it results in lowered to no inhibition. This phenomenon can be generalized for quantifiable inhibition by asRNAs on genomic targets. Meanwhile, another main contributor to determine inhibition efficiency is the relative abundance between asRNAs and targeted mRNAs, while the asRNA copy number needs to be at least comparable to its target for effective inhibition. We hypothesized that the inhibition level can be manipulated for genomic genes by altering the asRNA abundance and its targeting sequence around the core RBS region. To validate, we identified similar inhibition level gradients for the genomic targets *fabD* and *ydiI*. A mathematic model was established to describe such observations and successfully predicted the range and trend of the inhibition level change for both targets. We further demonstrated the regulatory effect of quantifiable inhibition levels on the biosynthesis of 4-HC. As expected, the different levels of inhibition on key reactions showed an influence on 4-HC titers, with up to a 3.58-fold increase. However, introducing more overexpressed genes dampened the regulatory effect of asRNAs, implying metabolic burden for extensively modified cells.

The titration of trans-acting elements such as asRNA and sRNA is essential for precise engineering of cells and has attracted attention only recently. As opposed to the current studies, we largely improved the resolution when mapping the extragenic regions, therefore quantified the asRNA-based inhibition levels when targeting around the core RBS region and developed a generalizable strategy that backed up by a mathematic model. A complementary strategy to achieve inhibition titration is through promoter engineering (Noh et al., 2017). Although effective, its application could be limited when the promoter sequences are challenging to be modified, such as in transcriptional factor-based biosensor systems. We believe our work will expedite the fine-tuning engineering efforts for asRNA design and provides fundamental knowledge in regulating the living systems.

Data availability

The raw data generated and analyzed during the current study are available from the corresponding author on reasonable request.

Code availability

The Matlab codes used in this study are available from the corresponding author on reasonable request.

Funding

CRediT authorship contribution statement

Ruihua Zhang: Conceptualization, Methodology, Software, Validation, Formal analysis, Investigation, Data curation, Writing, Writing – review & editing, Visualization, Supervision, Project administration, Funding acquisition. **Yan Zhang:** Investigation. **Jian Wang:** Writing – review & editing. **Yaping Yang:** Resources, Writing – review & editing. **Yajun Yan:** Conceptualization, Writing – review & editing.

Declaration of competing interest

The authors claim no conflict of interest.

Acknowledgment

Appendix A. Supplementary data

Supplementary data to this article can be found online at https://doi.org/10.1016/j.mec.2021.e00168.

Author contributions

R.Z. and YJ.Y. conceived the study and designed the experiments; R.Z. and Y.Z. conducted the experiments; J.W. and YP.Y. participated in discussion of the experiment design; YJ.Y. supervised the project; R.Z. wrote the manuscript; R.Z., J.W. and YJ.Y. revised the manuscript.

References

Aiba, H., 2007. Mechanism of RNA silencing by Hfq-binding small RNAs. Curr. Opin. Microbiol. 10, 134–139.

Baba, T., Ara, T., Hasegawa, M., Takai, Y., Okumura, Y., Baba, M., Datsenko, K.A., Tomita, M., Wanner, B.L., Mori, H., 2006. Construction of Escherichia coli K-12 in-frame, single-gene knockout mutants: the Keio collection. Mol. Syst. Biol. 2, 2006-0008.

Bailey, J.E., 1991. Toward a science of metabolic engineering. Science 252, 1668–1675.

Bremer, H., Dennis, P.P., 1996. Escherichia coli and Salmonella: Cellular and Molecular Biology. American Society for Microbiology. Chapter, Modulation of chemical composition and other parameters of the cell by growth rate, Washington (DC), pp. 1553–1569.

Chen, J.L., Dishler, A.L., Kennedy, S.D., Yildirim, I., Liu, B., Turner, D.H., Serra, M.J., 2012. Testing the nearest neighbor model for canonical RNA base pairs: revision of GU parameters. Biochemistry 51, 3508–3522.

Cho, S.H., Haning, K., Contreras, L.M., 2015. Strain engineering via regulatory noncoding RNAs: not a one-blueprint-fits-all. Current Opinion in Chemical Engineering 10, 25–34.

Cormack, B.P., Valdivia, R.H., Falkow, S., 1996. FACS-optimized mutants of the green fluorescent protein (GFP). Gene 173, 33–38.

Datsenko, K.A., Wanner, B.L., 2000. One-step inactivation of chromosomal genes in Escherichia coli K-12 using PCR products. Proc. Natl. Acad. Sci. Unit. States Am. 97, 6640–6645.

Gilbert, R., 2009. Physical Biology of the Cell, by Rob Phillips, Jane Kondev and Julie Theriot. Taylor & Francis, pp. 285–288.

Hebert, C.G., Valdes, J.J., Bentley, W.E., 2008. Beyond silencing—engineering applications of RNA interference and antisense technology for altering cellular phenotype. Curr. Opin. Biotechnol. 19, 500–505.

Hoynes-O'Connor, A., Moon, T.S., 2016. Development of design rules for reliable antisense RNA behavior in E. coli. ACS Synth. Biol. 5, 1441–1454.

Jing, P., Cao, X., Lu, X., Zong, H., Zhuge, B., 2018. Modification of an engineered Escherichia coli by a combined strategy of deleting branch pathway, fine-tuning xylose isomerase expression, and substituting decarboxylase to improve 1, 2, 4-butanetriol production. J. Biosci. Bioeng. 126, 547–552.

Lee, Y.J., Moon, T.S., 2018. Design rules of synthetic non-coding RNAs in bacteria. Methods 143, 58–69.

Lin, Y., Shen, X., Yuan, Q., Yan, Y., 2013. Microbial biosynthesis of the anticoagulant precursor 4-hydroxycoumarin. Nat. Commun. 4, 1–8.

Lutz, R., Bujard, H., 1997. Independent and tight regulation of transcriptional units in Escherichia coli via the LacR/O, the TetR/O and AraC/I1-I2 regulatory elements. Nucleic Acids Res. 25, 1203–1210.

Na, D., Yoo, S.M., Chung, H., Park, H., Park, J.H., Lee, S.Y., 2013. Metabolic engineering of Escherichia coli using synthetic small regulatory RNAs. Nat. Biotechnol. 31, 170–174.

Nakashima, N., Tamura, T., Good, L., 2006. Paired termini stabilize antisense RNAs and enhance conditional gene silencing in Escherichia coli. Nucleic Acids Res. 34 e138-e138.

Noh, M., Yoo, S.M., Kim, W.J., Lee, S.Y., 2017. Gene expression knockdown by modulating synthetic small RNA expression in Escherichia coli. Cell systems 5, 418–426 e414.

Park, H., Yoon, Y., Suk, S., Lee, J.Y., Lee, Y., 2014. Effects of different target sites on antisense RNA-mediated regulation of gene expression. BMB reports 47, 619–624.

Salis, H.M., 2011. Methods in Enzymology, vol. 498. Elsevier, pp. 19–42.

Salis, H.M., Mirsky, E.A., Voigt, C.A., 2009. Automated design of synthetic ribosome binding sites to control protein expression. Nat. Biotechnol. 27, 946–950.

Shaner, N.C., Campbell, R.E., Steinbach, P.A., Giepmans, B.N., Palmer, A.E., Tsien, R.Y., 2004. Improved monomeric red, orange and yellow fluorescent proteins derived from Discosoma sp. red fluorescent protein. Nat. Biotechnol. 22, 1567–1572.

Shen, X., Mahajani, M., Wang, J., Yang, Y., Yuan, Q., Yan, Y., Lin, Y., 2017. Elevating 4-hydroxycoumarin production through alleviating thioesterase-mediated salicoyl-CoA degradation. Metab. Eng. 42, 59–65.

Shen, X., Wang, J., Li, C., Yuan, Q., Yan, Y., 2019. Dynamic gene expression engineering as a tool in pathway engineering. Curr. Opin. Biotechnol. 59, 122–129.

Stephanopoulos, G., Vallino, J.J., 1991. Network rigidity and metabolic engineering in metabolite overproduction. Science 252, 1675–1681.

Sun, X., Shen, X., Jain, R., Lin, Y., Wang, J., Sun, J., Wang, J., Yan, Y., Yuan, Q., 2015. Synthesis of chemicals by metabolic engineering of microbes. Chem. Soc. Rev. 44, 3760–3785.

Tan, Y., Rivera, J.G.L., Contador, C.A., Asenjo, J.A., Liao, J.C., 2011. Reducing the allowable kinetic space by constructing ensemble of dynamic models with the same steady-state flux. Metab. Eng. 13, 60–75.

Tran, L.M., Rizk, M.L., Liao, J.C., 2008. Ensemble modeling of metabolic networks. Biophys. J. 95, 5606–5617.

Tummala, S.B., Welker, N.E., Papoutsakis, E.T., 2003. Design of antisense RNA constructs for downregulation of the acetone formation pathway of Clostridium acetobutylicum. J. Bacteriol. 185, 1923–1934.

Vogel, J., Luisi, B.F., 2011. Hfq and its constellation of RNA. Nat. Rev. Microbiol. 9, 578–589.

Wang, J., Mahajani, M., Jackson, S.L., Yang, Y., Chen, M., Ferreira, E.M., Lin, Y., Yan, Y., 2017. Engineering a bacterial platform for total biosynthesis of caffeic acid derived phenethyl esters and amides. Metab. Eng. 44, 89–99.

Wu, J., Yu, O., Du, G., Zhou, J., Chen, J., 2014. Fine-tuning of the fatty acid pathway by synthetic antisense RNA for enhanced (2S)-naringenin production from L-tyrosine in Escherichia coli. Appl. Environ. Microbiol. 80, 7283–7292.

Yang, Y., Lin, Y., Li, L., Linhardt, R.J., Yan, Y., 2015. Regulating malonyl-CoA metabolism via synthetic antisense RNAs for enhanced biosynthesis of natural products. Metab. Eng. 29, 217–226.

Yang, Y., Wang, J., Zhang, R., Yan, Y., 2019. Microbial Metabolic Engineering. Springer, pp. 23–35.

Yoo, S.M., Na, D., Lee, S.Y., 2013. Design and use of synthetic regulatory small RNAs to control gene expression in Escherichia coli. Nat. Protoc. 8, 1694–1703.

Zhang, R., Li, C., Wang, J., Yang, Y., Yan, Y., 2018. Microbial production of small medicinal molecules and biologics: from nature to synthetic pathways. Biotechnol. Adv. 36, 2219–2231.

Zuker, M., 2003. Mfold web server for nucleic acid folding and hybridization prediction. Nucleic Acids Res. 31, 3406–3415.